arXiv:1212.1267v2 [physics.atom-ph] 1 Mar 2013

Break up of Rydberg superatoms via dipole-dipole interactions

S. Möbius,[1] M. Genkin,[1] S. Wüster,[1] A. Eisfeld,[1] and J. M. Rost[1]

[1] *Max-Planck-Institute for the Physics of Complex Systems, 01187 Dresden, Germany*

(Dated: March 4, 2013)

We investigate resonant dipole-dipole interactions between two "superatoms" of different angular momentum, consisting of two Rydberg-blockaded atom clouds where each of them carries initially a coherently shared single excitation. We demonstrate that the dipole-dipole interaction breaks up the superatoms by removing the excitations from the clouds. The dynamics is akin to an ensemble average over systems where only one atom per cloud participates in entangled motion and excitation transfer. We also consider a modified setup, in which instead of a single shared Rydberg excitation each atom carries a small admixture of an excitation via off-resonant laser dressing. In this case, we observe collective motion for the entire cloud. This collective behavior constitutes a further step towards the implementation of entangled motional states. Moreover, our findings should facilitate the experimental realization of adiabatic exciton transport in Rydberg systems by replacing single sites with atom clouds.

PACS numbers: 32.80.Ee, 34.20.Cf, 82.20.Rp

I. INTRODUCTION

Rydberg atoms have several remarkable properties, such as long lifetimes, large polarizability and strong long-range interactions. These properties have turned Rydberg atoms into versatile tools for quantum information [1–5], nonlinear quantum optics [6–8] or cavity quantum electrodynamics [9–11]. Recently, also the potential of Rydberg atoms for quantum transport in atomic aggregates has been demonstrated [12–16]. The underlying physical mechanism is closely related to the one of excitation transport in molecular systems [13, 17, 18].

So far, only single atoms have been considered as building blocks for excitation transport in Rydberg aggregates. An experimental implementation would be facilitated if the single atom sites could be replaced by atom clouds. This has motivated us to explore the possibilities for extending the existing Rydberg transport schemes using atom clouds as sites.

When several atoms are brought together in clouds, they exhibit an effect known as Rydberg blockade [19–28]. At small interatomic distances, the van-der-Waals interactions $U_{\mathrm{vdW}} = C_6/r^6$ (where C_6 is a state-dependent interaction constant and r the interatomic distance) become large. These interactions lead to an energy offset of all many-particle states with more than one Rydberg excitation with respect to the energy of the states with just a single excitation. As a consequence, although irradiating an entire atomic cloud, a laser can create at most one Rydberg excitation resonantly, within a radius at which this energy offset is larger than the laser linewidth. The latter is limited by the Rabi frequency Ω of the driven transition, which gives an estimate of the minimum interatomic distance between two Rydberg excitations, known as the blockade radius $r_{\mathrm{bl}} \approx (C_6/\hbar\Omega)^{1/6}$. The interplay of the Rydberg blockade with quantum transport has appealing new aspects which we investigate in the following.

We concentrate on a system of two atom clouds, well separated in space. A similar arrangement was studied in Ref. [29] in the limit of a frozen Rydberg gas. Here we choose the spatial extension σ of each cloud to be smaller than the blockade radius r_{bl}, while the inter-cloud distance L is significantly larger than r_{bl}, see Fig. 1. For such parameters, the electron dynamics is restricted to a single Rydberg excitation per cloud, and we consider a situation in which each of the two Rydberg-blockaded clouds is initially prepared in a coherent collective excitation. Such states can nowadays be experimentally created [24] and are sometimes referred to as superatoms [30, 31]. They are a coherent superposition of states where all atoms within the cloud but one are in the ground state and one atom is in a Rydberg state $|\nu l\rangle$. Here, ν and l denote the principal and angular momentum quantum numbers of the Rydberg state, respectively. We shall further imply with the term superatom, that all the atoms taking part in the superposition of electronic states share almost identical spatial probability distributions.

We will analyze the resonant dipole-dipole interactions [32–34] between two superatoms of different angular momentum, with the setup and the model described in section II. Then, we will discuss the electronic excitation transfer in the limit of frozen atomic positions in section III, which already singles out some interesting features of the two interacting superatoms. Subsequently, we will turn to the effects of the electronic excitations on the motion of the atoms in section IV. Finally, in section V, we will investigate how the character of the dynamics changes, if Rydberg-dressed [35–38] ground state atoms are considered instead of an actual Rydberg excitation. The paper ends with a summary and conclusion in section VI.

II. THE SETUP

We denote the two atom clouds as A and B with N_A and N_B atoms in the respective cloud, while $N = N_A + N_B$ is the total number of atoms. Each atom is labeled uniquely, such that atoms with numbers $1..N_A$ belong to cloud A while $(N_A + 1)..N$ refers to atoms in cloud B, summarized in the index sets

$$\mathcal{A} = [1, .., N_A], \quad \mathcal{B} = [N_A + 1, .., N]. \tag{1}$$

We consider one spatial dimension along the separation of the clouds, and take three electronic states into account: The ground state $|g\rangle$ and two Rydberg states $|\nu s\rangle$ and $|\nu p\rangle$. Since the principal quantum number ν of the Rydberg states is kept fixed it will be omitted in the following. With these restricitions, the Hamiltonian for our system reads

$$H(r_1, ..., r_N) = -\sum_{i=1}^{N} \frac{\hbar^2}{2M} \nabla_{r_i}^2 + H_{\rm el}(r_1, ..., r_N), \tag{2}$$

where M is the mass of a single atom, r_i the position of the i-th atom and $H_{\rm el}$ the electronic Hamiltonian describing dipole-dipole-interactions between the atoms. Generally, any of the N atoms can be in either of the three states $|g\rangle$, $|s\rangle$, $|p\rangle$. However, the Rydberg blockade and the binary character of the dipole-dipole interactions significantly reduce the dimensionality of our problem. The former excludes states with more than one Rydberg excitation with *the same* angular quantum number within one cloud, while the latter excludes states in which both the s *and* the p excitation are localized within one cloud. We define electronic states

$$|\pi_{nm}\rangle = |ggg..s..ggg..p..ggg\rangle \tag{3}$$

where the n-th atom is in the Rydberg state $|s\rangle$, the m-th atom in the Rydberg state $|p\rangle$ and all others in the ground state, and impose and additional constraint

$$(n \in \mathcal{A} \text{ and } m \in \mathcal{B}) \text{ OR } (m \in \mathcal{A} \text{ and } n \in \mathcal{B}), \tag{4}$$

as sketched in Fig. 1. The states of Eq. (3) constrained according to Eq. (4) thus constitute a basis in the $2N_AN_B$-dimensional electronic subspace. We assume that the dipole-dipole interaction of strength V_0

$$V_{nm}(r_{nm}) = \frac{V_0}{r_{nm}^3} \tag{5}$$

between the two excited atoms n and m depends only on the interatomic distance $r_{nm} = |r_n - r_m|$ neglecting possible orientation effects. This is a sufficient description for certain geometries and selected states [16, 29, 39]. Using Eq. (5) the matrix elements of the electronic Hamiltonian $H_{\rm el}$ from Eq. (2) read

$$\langle \pi_{nm} | \, H_{\rm el} \, |\pi_{n'm'}\rangle = V_{nm} \delta_{nm'} \delta_{mn'}. \tag{6}$$

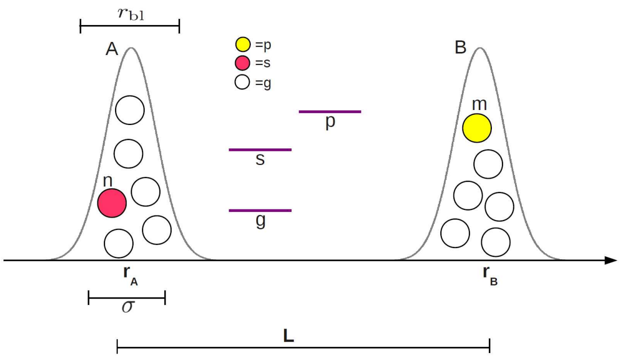

FIG. 1: Color online: Sketch of two interacting Rydberg blockaded clouds (not drawn to scale). The width σ of the Gaussian distribution of the atoms within each cloud is smaller than the blockade radius $r_{\rm bl}$, while the distance L between the clouds is larger. The coloring (shading) illustrates the electronic basis states $|\pi_{nm}\rangle$ introduced in Eq. (3).

TABLE I: Matrix elements of the electronic Hamiltonian $H_{\rm el}$ in the basis $|\pi_{nm}\rangle$ for the example of $N_A = N_B = 2$.

$H_{\rm el}$	$\|\pi_{13}\rangle$	$\|\pi_{31}\rangle$	$\|\pi_{14}\rangle$	$\|\pi_{41}\rangle$	$\|\pi_{23}\rangle$	$\|\pi_{32}\rangle$	$\|\pi_{24}\rangle$	$\|\pi_{42}\rangle$
$\langle\pi_{13}\|$	0	V_{13}	0	0	0	0	0	0
$\langle\pi_{31}\|$	V_{13}	0	0	0	0	0	0	0
$\langle\pi_{14}\|$	0	0	0	V_{14}	0	0	0	0
$\langle\pi_{41}\|$	0	0	V_{14}	0	0	0	0	0
$\langle\pi_{23}\|$	0	0	0	0	0	V_{23}	0	0
$\langle\pi_{32}\|$	0	0	0	0	V_{23}	0	0	0
$\langle\pi_{24}\|$	0	0	0	0	0	0	0	V_{24}
$\langle\pi_{42}\|$	0	0	0	0	0	0	V_{24}	0

As a consequence of the Rydberg blockade, the electronic Hamiltonian in the matrix representation, Eq. (6), has a block-diagonal structure, as can be seen in Table I. This has drastic consequences for the electron and atom dynamics: (i) The excitation exchange between the clouds can be resembled by an average over single atom pairs and (ii) the force resulting from the dipole-dipole interactions only acts on one atom rather than the whole cloud. We will discuss these effects in sections III and IV, respectively.

The full wave function can be written as an expansion in the electronic basis $|\pi_{nm}\rangle$

$$|\, \Psi(\mathbf{R}, t)\, \rangle = \sum_{nm} \phi_{nm}(\mathbf{R}, t) |\pi_{nm}\rangle \tag{7}$$

with coefficients $\phi_{nm}(\mathbf{R}, t)$ which depend on time t and the atomic positions r_i, summarized in the vector $\mathbf{R} = (r_1, .., r_N)$. The probability to find an s-excitation on atom n and a p-excitation on atom m is given by

$$P_{nm}(t) = \int d^N\mathbf{R}\, |\phi_{nm}(\mathbf{R},t)|^2. \tag{8}$$

Often the initial state of the system can be written as a direct product

$$|\,\Psi^{\rm ini}\,\rangle = |\,\psi_{\rm el}^{\rm ini}\,\rangle \otimes |\,\chi_{\rm sp}^{\rm ini}\,\rangle, \tag{9}$$

where $|\,\psi_{\rm el}^{\rm ini}\,\rangle$ is the initial electronic state and $|\,\chi_{\rm sp}^{\rm ini}\,\rangle$ the initial wave function of the atoms. The latter is taken as a product of one-dimensional Gaussians in position space, centered around the respective centers r_A, r_B of the two clouds,

$$\chi_{\rm sp}^{\rm ini}(\mathbf{R}) = \prod_{n=1}^{N_A} \chi_1^\sigma(r_n - r_A) \prod_{n=N_A+1}^{N} \chi_1^\sigma(r_n - r_B), \tag{10}$$

where

$$\chi_{\mathcal{D}}^\sigma(\mathbf{x}) = \left(\pi\sigma^2\right)^{-\mathcal{D}/4} \exp\left(-|\mathbf{x}|^2/2\sigma^2\right) \tag{11}$$

denote a Gaussian in $\mathcal{D}$ dimensions. The width σ is taken such that $\sigma < r_{\rm bl}$ and $\sigma \ll L$, where $L = |r_A - r_B|$ is the distance between the clouds. This choice of the initial spatial wave function models an experimental preparation of the atoms in the lowest oscillator states of two harmonic traps. Our initial electronic wave function $|\,\psi_{\rm el}^{\rm ini}\,\rangle$ is taken to represent a superatom state in both clouds. Specifically, all atoms in cloud A coherently share the Rydberg s-excitation and all atoms in cloud B coherently share the Rydberg p-excitation:

$$|\,\psi_{\rm el}^{\rm ini}\,\rangle = \frac{1}{\sqrt{N_A N_B}} \sum_{n\in\mathcal{A},\, m\in\mathcal{B}} |\pi_{nm}\rangle. \tag{12}$$

Note that the position-dependent dipole-dipole potential entangles the electronic interactions and atomic motion [14–16, 40], so that for $t > 0$ the direct product form of the wave function will not persist.

III. DYNAMICS IN THE ELECTRONIC SUBSPACE

Before tackling the intricate interplay of electronic excitation and atom motion, we first study purely electronic dephasing of population oscillations arising from the initial state, Eq. (12). The observable of interest is P_A^s, the s-population in cloud A, which can be defined in terms of the occupations of the electronic states (cf. Eq. (8)) as

$$P_A^s(t) = \sum_{n\in\mathcal{A}\, m\in\mathcal{B}} P_{nm}(t). \tag{13}$$

For our initial state (Eq. (12)) we have $P_A^s(t=0) = 1$. Due to the interactions (Eq. (5)), the s-population will migrate from cloud A to cloud B, while p-population will migrate from cloud B to cloud A, resulting in Rabi-oscillations of the quantity $P_A^s(t)$. The oscillations dephase due to the width of the initial spatial wave functions $|\,\chi_{\rm sp}^{\rm ini}\,\rangle$. In this section, we will show that this behavior can be understood already within a semiclassical picture. Moreover, we will also show that the same dephasing can be equivalently obtained as an effect of disorder by statistically avering over fixed point particles.

For the following semiclassical treatment, it is convenient to represent the electronic subspace in the basis of the eigenstates $|\varphi_k(\mathbf{R})\rangle$ of the electronic Hamiltonian, rather than in the basis $|\pi_{nm}\rangle$ introduced in Eq. (3). These states satisfy

$$H_{\rm el}(\mathbf{R})|\varphi_k(\mathbf{R})\rangle = U_k(\mathbf{R})|\varphi_k(\mathbf{R})\rangle, \tag{14}$$

and the wave function is expanded as

$$|\,\Psi(\mathbf{R},t)\,\rangle = \sum_k \tilde{\phi}_k(\mathbf{R},t)|\varphi_k(\mathbf{R})\rangle. \tag{15}$$

We call the eigenenergies $U_k(\mathbf{R})$ (adiabatic) potential energy surfaces and $\tilde{\phi}_k(\mathbf{R},t)$ spatial wave functions in the adiabatic representation [14, 41]. The index k runs over the $2N_AN_B$ dimensions of the electronic subspace. For an electronic Hamiltonian with the structure of Eq. (6) (see also Table I), the mapping of the basis functions from the expansion in Eq. (7), $|\pi_{nm}\rangle$, onto the adiabatic basis $|\varphi_k(\mathbf{R})\rangle$, Eq. (15), is particularly simple. The eigenvalues U_k, $k = 1,..,2N_AN_B$ of the electronic Hamiltonian can be grouped into N_AN_B pairs, each of which can be written in terms of the Hamiltonian matrix elements as $U_{nm}^\pm(\mathbf{R}) = \pm V_{nm}(r_{nm})$, cf. Eq. (6). Similarly, the corresponding eigenvectors have the form $|\varphi_{nm}^\pm\rangle = (|\pi_{nm}\rangle \pm |\pi_{mn}\rangle)/\sqrt{2}$. Therefore, we can rewrite the adiabatic expansion from Eq. (15) as

$$|\,\Psi(\mathbf{R},t)\,\rangle = \sum_{n\in\mathcal{A},m\in\mathcal{B}} \left(\tilde{\phi}_{nm}^+(\mathbf{R},t)|\varphi_{nm}^+\rangle + \tilde{\phi}_{nm}^-(\mathbf{R},t)|\varphi_{nm}^-\rangle\right). \tag{16}$$

The equations of motion for the coefficients $\tilde{\phi}_{nm}^\pm$ are then obtained from the time-dependent Schrödinger equation and read

$$i\hbar\frac{\partial}{\partial t}\tilde{\phi}_{nm}^\pm(\mathbf{R},t) = -\sum_{i=1}^{N}\frac{\hbar^2}{2M}\nabla_{r_i}^2\tilde{\phi}_{nm}^\pm(\mathbf{R},t) + U_{nm}^\pm(r_{nm})\tilde{\phi}_{nm}^\pm(\mathbf{R},t). \tag{17}$$

Since the above equations decouple for different atom pairs nm and surfaces $\pm$, we can solve them separately and will often suppress the indices nm in the remainder of this section. In the following two subsections, we will introduce a semiclassical propagator and show that the latter yields dephasing oscillations of P_A^s (subsection III A), which agree with a full quantum mechanical calculation. In subsection III B, we demonstrate that exactly the same dephasing oscillations arise even if the atoms are treated as fixed classical point particles. Together, subsections III A and III B rigorously justify the use of the frequently employed so-called frozen gas approximation for our scenario. The reader content with its applicability may thus directly proceed to the semiclassical expression for $P_A^s(t)$ in Eq. (31).

A. Semiclassical treatment

Now we introduce the semiclassical approach. We choose the Herman-Kluk propagator K^{HK} in the initial value representation [42–45], that achieves

$$\tilde{\phi}^{\pm}(\mathbf{R}'',t) = \int d\mathbf{R}' K^{HK}(\mathbf{R}'',t;\mathbf{R}',t{=}0)^{\pm}\tilde{\phi}^{\pm}(\mathbf{R}',t{=}0). \tag{18}$$

The propagation is carried out in terms of multiple classical initial value solutions and trajectory averaging. Such an approach constitutes a useful numerical method; Here, however, we shall use it for some simplifying theoretical arguments.

The propagator reads

$$\begin{aligned} &K^{HK}(\mathbf{R}'',t;\mathbf{R}',t{=}0)^{\pm} = \\ &\int \frac{d^N p' d^N q'}{(2\pi\hbar)^N} \langle\, \mathbf{R}'' \,|\, z_t \,\rangle C(\mathbf{q}_t,\mathbf{p}_t,\mathbf{q}',\mathbf{p}') \\ &\times \exp\left(\frac{i}{\hbar} S^{\pm}[\mathbf{q}_t,\mathbf{p}_t] - \frac{i}{2\hbar}(\mathbf{q}_t\mathbf{p}_t - \mathbf{q}'\mathbf{p}')\right) \langle\, z' \,|\, \mathbf{R}' \,\rangle. \end{aligned} \tag{19}$$

Here, $|\, z' \,\rangle$ are coherent states centered on position $\mathbf{q}'$ and momentum $\mathbf{p}'$,

$$\langle\, \mathbf{R} \,|\, z' \,\rangle = \chi_N^{\sigma_0}(\mathbf{R} - \mathbf{q}') \exp\left[\frac{i}{\hbar}\mathbf{p}'\left(\mathbf{R} - \frac{\mathbf{q}'}{2}\right)\right], \tag{20}$$

with χ_N^{σ} defined in Eq. (11). The width σ_0 of these states is just a numerical parameter, which is adapted to the given problem. For simplicity, in the following we set it to be equal to the width of the initial wave function defined in Eq. (10), i.e. $\sigma_0 = \sigma$. The expressions $\mathbf{q}_t$, $\mathbf{p}_t$ are trajectories evolved with the classical Hamiltonian $H_{\mathrm{c}} = \mathbf{p}_t^2/2M + U^{\pm}(\mathbf{q}_t)$ from the initial conditions $\mathbf{q}'$, $\mathbf{p}'$. We denote the classical action along these trajectories by $S^{\pm}[\mathbf{q}_t,\mathbf{p}_t] = \int [\mathbf{p}_t^2/2M - U^{\pm}(\mathbf{q}_t)]dt$. The time-dependent coherent states centered around the phase space trajectories $\mathbf{q}_t$, $\mathbf{p}_t$ are labeled by $|\, z_t \,\rangle$. Finally, the prefactor C is defined by the trajectories as

$$C = \left| \frac{1}{2}\left(\frac{\partial \mathbf{p}_t}{\partial \mathbf{p}'} + \frac{\partial \mathbf{q}_t}{\partial \mathbf{q}'} - \frac{i\hbar}{\sigma^2}\frac{\partial \mathbf{q}_t}{\partial \mathbf{p}'} - \frac{\sigma^2}{i\hbar}\frac{\partial \mathbf{p}_t}{\partial \mathbf{q}'} \right) \right|^{\frac{1}{2}}. \tag{21}$$

In Appendix A, we show step by step that under certain conditions, the form of the propagator (19) can be substantially simplified. The conditions are (i) $L \gg \sigma$, (ii) the dynamics is considered only on sufficiently short timescales, and (iii) the classical kinetic energy $E_k^c = \mathbf{p}_t^2/2M$ on these timescales is negligible compared to the potential energy $E_p^c = U^{\pm}(\mathbf{q}_t)$. The timescale is essentially defined by the ratio (L/σ) and the inverse uncertainty of the potential energy, i.e. we restrict ourselves to times

$$t \ll \frac{L}{\sigma}\frac{\hbar}{\Delta E_p} \tag{22}$$

where the uncertainty of the potential energy is estimated as

$$\Delta E_p \approx \left| \frac{\partial V_{nm}(r_{nm})}{\partial r_{nm}} \right| \sigma \approx \left| \frac{3V_0\sigma}{L^4} \right|. \tag{23}$$

With these conditions, as shown in Appendix A, the Herman-Kluk propagator becomes

$$K^{HK}(\mathbf{R}'',t;\mathbf{R}',t{=}0)^{\pm} = \exp\left[-\frac{it}{\hbar}U^{\pm}(\mathbf{R}')\right]\delta(\mathbf{R}' - \mathbf{R}''). \tag{24}$$

Hence, the time-propagated adiabatic spatial wave function is given by

$$\tilde{\phi}^{\pm}(\mathbf{R}'',t) = \exp\left[-\frac{it}{\hbar}U^{\pm}(\mathbf{R}'')\right]\tilde{\phi}^{\pm}(\mathbf{R}'',t{=}0). \tag{25}$$

This result is equivalent to the solution of the Eqs. (17) if, in the latter, the kinetic energy operator is ignored.

Now recall that the adiabatic surfaces $U^{\pm}(\mathbf{R}'') = U^{\pm}_{nm}(\mathbf{R}'')$ not only depend on just two coordinates r_n, r_m, but actually solely on the relative coordinate $r_{nm} = r_n - r_m$. Further, as already mentioned, the equations of motion for the adiabatic wave functions decouple for different atom pairs. We can thus without loss of generality restrict our treatment to a single atom pair nm und transform the wave function onto relative and center of mass coordinates:

$$r_{nm} = r_n - r_m, \quad R^{CM}_{nm} = \frac{r_n + r_m}{2}. \tag{26}$$

After separating the center of mass motion, the dynamics becomes effectively one-dimensional. From the initial state (Eqs. (9,10)), we obtain

$$\tilde{\phi}^{\pm}_{nm}(r_{nm},t{=}0) = \frac{1}{\sqrt{2}}\chi_1^{\sqrt{2}\sigma}(r_{nm} - L), \tag{27}$$

with $\chi_1^{\sqrt{2}\sigma}$ as defined in Eq. (11). The width $\sqrt{2}\sigma$ results from the transformation onto the relative coordinate, while the additional $1/\sqrt{2}$ factor follows from our normalization convention in the adiabatic expansion. The Herman-Kluk propagation (24) therefore yields

$$\tilde{\phi}^{\pm}_{nm}(r_{nm},t) = \frac{1}{\sqrt{2}}\exp\left[\mp\frac{it}{\hbar}\frac{V_0}{r^3_{nm}}\right]\chi_1^{\sqrt{2}\sigma}(r_{nm} - L). \tag{28}$$

The s-population in cloud A in the semiclassical picture $P^{sc}_{s,A}$ for a single atom pair nm can be extracted from the spatial wave function in the adiabatic representation as

$$P^{sc}_{s,A}(t) = \frac{1}{2}\int \mathrm{d}r_{nm} \left| \tilde{\phi}_{nm}(r_{nm},t)^{+} + \tilde{\phi}_{nm}(r_{nm},t)^{-} \right|^2. \tag{29}$$

Inserting the Herman-Kluk-propagated wave functions from Eq. (28) leads to the expression

$$P^{sc}_{s,A}(t) = \left(\frac{2}{\pi\sigma^2}\right)^{1/2} \int \mathrm{d}L' \cos^2\left(\frac{V_0 t}{\hbar L'^3}\right) \exp\left[-\frac{(L'-L)^2}{2\sigma^2}\right]. \tag{30}$$

This integral cannot be solved analytically exactly, but by substituting $\eta = L - L'$ and Taylor-expanding $(L+\eta)^{-3} \approx L^{-3}(1-3\eta/L)$ one finds the following approximate solution for the s-population in cloud A:

$$P^{sc}_{s,A}(t) = \frac{1}{2}\left[1 + \cos(\omega t)\exp\left(-\left(\frac{3\sigma}{\sqrt{2}L}\omega t\right)^2\right)\right], \tag{31}$$

with $\omega = (2V_0/L^3)/\hbar$. We thus observe superexponentially dephasing Rabi-oscillations already within the semi-classical picture, where the dephasing time is determined by the ratio σ/L:

$$\tau_{\mathrm{deph}} = \frac{\sqrt{2}L}{3\sigma\omega} = \frac{\sqrt{2}\hbar L^4}{6\sigma V_0}. \tag{32}$$

This dephasing time is always within the timescale $\tau_{\mathrm{deph}} \ll (L/\sigma)^2 \hbar L^3/(3V_0)$ as long as $\sigma \ll L$, which is consistent with the conditions initially imposed for the semiclassical treatment, cf. Eq. (22).

B. Classical point particle limit

Let us finally remark that it is, in fact, possible, to arrive at the very same expression by an even cruder approximation, namely by simply describing the atoms as fixed point particles and averaging over their positions. In such a picture, there is no dynamics in position space and the expansion of the wave function in terms of the basis $|\pi_{nm}\rangle$ as given in Eq. (7) can be simply written as

$$|\,\Psi(t)\,\rangle = \sum_{nm} f_{nm}(t)|\pi_{nm}\rangle. \tag{33}$$

The expansion coefficients f_{nm} evolve according to

$$i\hbar\frac{\partial}{\partial t} f_{nm}(t) = V_{nm}(r_{nm}) f_{mn}(t). \tag{34}$$

Consequently, the s-population in cloud A in the point particle limit is given by

$$\mathcal{P}^s_A(t) = \sum_{n\in\mathcal{A}\, m\in\mathcal{B}} |f_{nm}(t)|^2. \tag{35}$$

Let us first consider the simplest case $N_A = 1$ and $N_B = 1$ to determine the probability to find the s–excitation at time t on the atom in cloud A. Eq. (34) can be solved to give non-dephasing Rabi oscillations

$$p_k(t) = |\langle\pi_{12}|\Psi(t)\rangle|^2 = |f_{12}(t)|^2 = \cos^2\left(\frac{V_0 t}{d_k^3\hbar}\right), \tag{36}$$

where d_k denotes the distance between the two atoms, in a particular stochastic realisation k of the atomic spatial distribution. Averaging this function over a large number G of realizations yields the expression for the s-population for point-like, fixed atoms,

$$\bar{p}(t) = \frac{1}{G}\sum_{k=1}^{G} p_k(t). \tag{37}$$

The expression does not change for the general case $N_A > 1$, $N_B > 1$: From the block structure of the electronic Hamiltonian, one can infer that the averaged result is exactly the same as in the case $N_A = 1$ and $N_B = 1$, we simply have added to the average over positions an average over blocks, which has exactly the same structure. In the limit $G \to \infty$, the sum in the above expression becomes an integral, in which the distances d_k follow the initial spatial distribution. This gives precisely the same expression as in Eq. (31). In Fig. 2, we demonstrate the agreement between the exact quantum mechanical result and the point particle limit, where the latter is also shown for a larger number of atoms ($N = 20$).

In summary, due to the particular structure of H_{el}, the time evolution of electronic populations per cloud for arbitrary N_A, N_B is identical to the average over an ensemble of systems with $N_A = N_B = 1$. We explicitly demonstrated this using a point particle model, and further argue in Appendix B that this behaviour will persist fully quantum mechanically. Note, however, that while the point particle approximation gives a correct description for the specific case studied here, it will in general give different results than a full quantum mechanical treatment. As an example, consider a setup in which the two clouds are additionally confined in two strong harmonic traps with energy spacing $\Delta E \gg V_0/L^3$. In this case the kinetic energy term is by construction much larger than the dipole-dipole interaction. Then, in a quantum treatment, $P^s_A(t)$ would undergo long coherent oscillations without dephasing, while an average over point particles would show fast dephasing as without the traps.

IV. ATOMIC MOTION

We now extend our calculations to timescales on which the dipole-dipole-induced atomic motion becomes clearly visible. Although the motion of the atoms is restricted to one dimension along the separation of the clouds, the full many-body problem is still too complex to be treated fully quantum mechanically. Therefore, we use a quantum-classical hybrid approach, which has been successfully applied to similar systems [14–16], namely Tully's fewest switching algorithm [46–48]. The method relies on a classical treatment of the atomic trajectories and a quantum mechanical treatment of the electronic degrees of freedom. A detailed description can be found in the aforementioned references, and we only briefly sum-

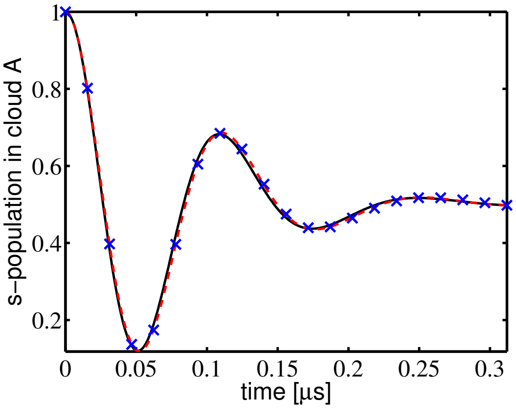

FIG. 2: Color online. S-population in cloud A as a function of time, shown for $N_A = N_B = 1$ fully quantum mechanically ($P_A^s(t)$, Eq. (13), solid black line), as an average over point particles ($\bar{p}(t)$, Eq. (37), red dashed line, for $N_A = N_B = 1$), and as an average over point particles for $N_A = N_B = 10$ (crosses). The following parameters were used: $\sigma = \sqrt{2}/3\,\mu$m, $L = 6\,\mu$m, $V_0 = 10^6$ a.u., corresponding to Li atoms with the principal quantum number $\nu \approx 30..40$, and $M = 11000$ a.u. (mass of ^{6}Li).

marize the main aspects relevant for the present problem in Appendix C.

The results of the simulations are shown in Fig. 3. We observe that, although the initial Rydberg excitation is coherently shared by all atoms within one cloud, it is nevertheless just a single atom that is ejected from each cloud. The atoms are still in a coherent superposition where *each of them* has left its cloud with some probability, but the ejected atoms always carry the excitation and an ensemble of ground-state atoms stays behind. In this sense the superatoms break apart when subject to dipole-dipole induced motion, since excited and ground-state atoms are now spatially separated.

Another interesting aspect is that the resulting motion is a superposition of repulsion and attraction. It is known [14] that for single Rydberg atoms interacting via dipole-dipole-forces, the direction of the force can be controlled via the initial electronic state; The same holds for our system, i.e. the choice of $|\,\psi_{\rm el}^{\rm ini}\,\rangle$ in Eq. (12) determines the motional dynamics. For $V_0 > 0$, the initial electronic states

$$|\,\psi_{\rm el}^{\pm}\,\rangle = \frac{1}{\sqrt{2N_A N_B}} \sum_{n\in\mathcal{A},\, m\in\mathcal{B}} \left(|\pi_{nm}\rangle \pm |\pi_{mn}\rangle\right) \qquad (38)$$

correspond to purely attractive (+) and repulsive (-) motion of the atom pair. The initial state chosen in Eq. (12), describing two superatoms, is a superposition of these two states, and consequently leads to a superposition of two opposite motion directions.

The presented results have interesting implications for quantum transport protocols based on single-atomic aggregates, such as adiabatic entanglement transport [15, 16]. Our findings show that even in an ensemble of atoms which share the Rydberg excitation, only one of them will be set in motion by dipole-dipole forces. This facilitates the experimental realization of transport schemes in [15, 16], since there is apparently no need to isolate single atoms. As formally discussed in Appendix B, our results can be extended to more than two clouds, due to the block structure of the full Hamiltonian, Eq. (2), and the corresponding time evolution operator $U(t) = \exp\left[-iHt\right]$. A 'Gedankenexperiment' presenting the transport scheme of Refs. [15, 16] both, with single atoms and with atoms clouds, is sketched in Fig. 4. If atom clouds are used one should consider that the transport efficiency may be affected by collisions of moving Rydberg atoms with resting ground state atoms for a large number of atoms per cloud. However, as estimated in Appendix D, in an ultracold gas such processes can

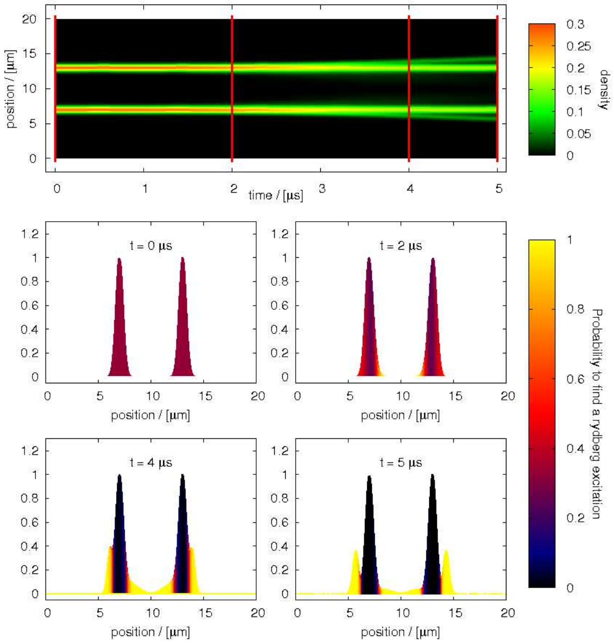

FIG. 3: Color online. Atomic motion induced by dipole-dipole interactions. The upper panel shows the atomic density as a function of time. The lower four panels show snapshots of the density at times $t = 0, 2, 4, 5\,\mu$s. The color indicates the probability to find any Rydberg excitation ($|s\rangle$ or $|p\rangle$) at a given position. In this figure, we do not distinguish between $|s\rangle$ and $|p\rangle$ excitations, since the dephasing oscillations of electronic population, as shown in Fig. 2, occur on the short timescale $t \sim 0.2\,\mu$s and are therefore not shown here. We observe that the main bulk of the atoms remains at rest, with vanishing probability to find an excitation. A pair of single atoms is ejected, and the Rydberg excitation is entirely localized on those two atoms. The calculations are shown for $N_A = N_B = 3$, for the same parameters as in Fig. 2 but with $M = 12600$ a.u., corresponding to the mass of ^{7}Li.

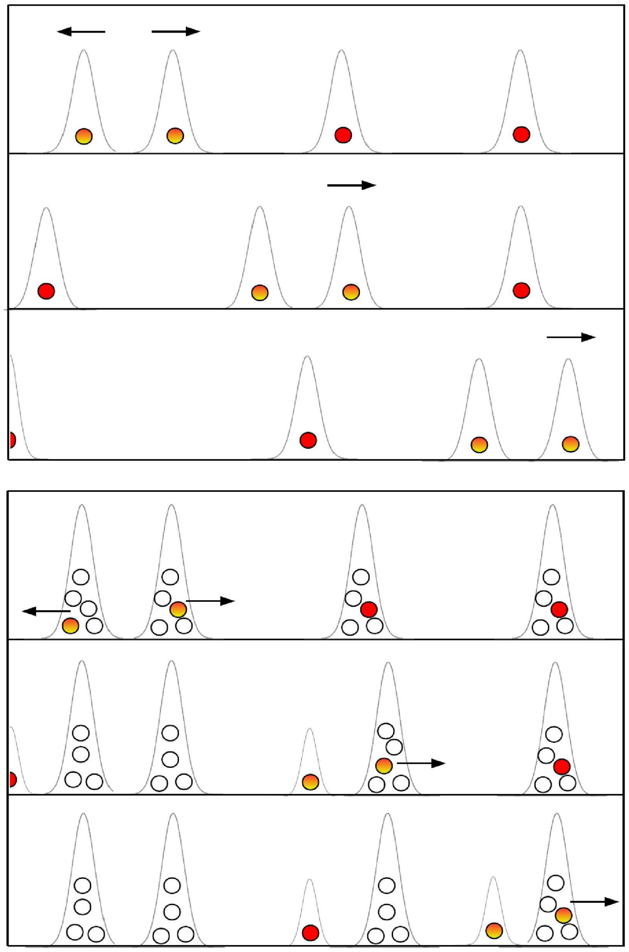

FIG. 4: Color online. Sketch of the excitation transport scheme with atom clouds as sites (lower panel), compared to the one with single atom sites (upper panel) as demonstrated in Refs. [15, 16]. Color codes are as in Fig. 1. All but one atom from each cloud remain at rest and do not participate in the dynamics, hence excitation and entanglement transport occur equivalently in both schemes. For the sake of clarity, the lower panel shows the dynamics for a well defined choice of initially excited atoms in each cloud, while the complete dynamics consists of a superposition where each atom in each cloud has the chance to be the only one from that cloud participating in the dynamics.

be neglected on the microsecond timescale. Before concluding this section, we also mention that the validity of the adopted quantum-classical hybrid approach was verified by comparing the time evolution of the spatial probability density with a full quantum calculation for the accessible case $N_A = N_B = 2$, as demonstrated in Fig. 5.

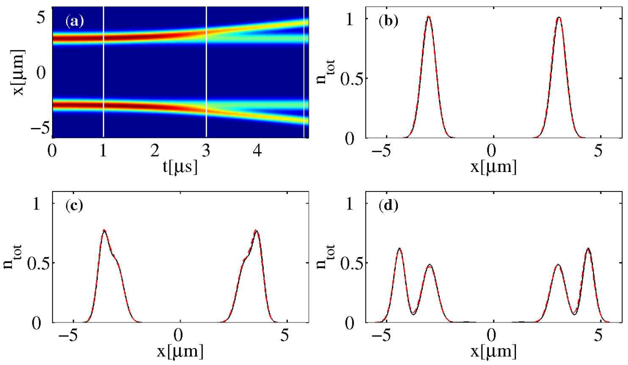

FIG. 5: Color online. Comparison of the atom density during superatom break-up, obtained from a full quantum mechanical calculation using Eq. (17) (solid black line) and Tully's quantum-classical hybrid algorithm (red dashed line). (a) Total atom density as a function of time. (b)-(d): Snapshots at three different times, as indicated by white vertical lines in (a): $t_1 = 1\,\mu$s (b), $t_2 = 3\,\mu$s (c), $t_3 = 4.9\,\mu$s (d). The same parameters as in Fig. 2 were used. For the sake of clarity, the comparison is shown for an initially purely repulsive electronic state, cf. Eq. (38).

V. AVOIDING THE BREAK-UP: RYDBERG DRESSING

In the previous section, we demonstrated that dipole-dipole interactions between superatoms do not lead to their collective motion. In this section, we will show that the situation is quite different for essentially the same setup but using Rydberg-dressed ground state atoms [38].

For each atom, we now take into account two hyperfine ground states $|g\rangle$, $|h\rangle$ and two Rydberg states $|s\rangle$, $|p\rangle$. Using off-resonant dressing lasers fields, we selectively couple $|g\rangle$ to $|s\rangle$ and $|h\rangle$ to $|p\rangle$. The corresponding Rabi frequencies and detunings are denoted by Ω_s, Ω_p and Δ_s, Δ_p respectively, see Fig. 6 and Ref. [38]. For simplicity, we take here the Rabi frequencies and detunings to be the same for both transitions,

$$\Omega_s = \Omega_p = \Omega, \quad \Delta_s = \Delta_p = \Delta. \tag{39}$$

The dressing lasers lead to a small admixture of the excited states to the ground states, giving rise to dressed states

$$|\,\tilde{g}\,\rangle = \mathcal{N}(|\,g\,\rangle + \alpha|\,s\,\rangle, \quad |\,\tilde{h}\,\rangle = \mathcal{N}(|\,h\,\rangle + \alpha|\,p\,\rangle), \tag{40}$$

where $\alpha = \Omega/(2\Delta) \ll 1$ is a dimensionless scaling parameter and $\mathcal{N}$ a normalisation factor. As shown in Ref. [38], the dressing lasers lead to an effective interaction Hamiltonian

$$\hat{H}_{\text{eff}} = \tilde{V}_{12}|\tilde{g}\rangle_1|\tilde{h}\rangle_2\langle\tilde{h}|_1\langle\tilde{g}|_2, \tag{41}$$

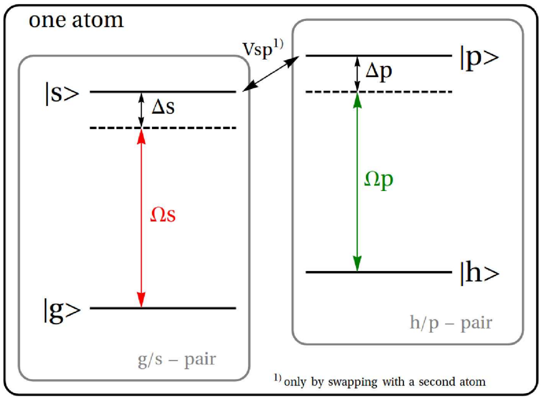

FIG. 6: Color online. General scheme of the dressing mechanism. Only one atom is shown. For a transition, a second one with the reverse process is needed. The effective interaction between two atoms in dressed ground states $|\tilde{g}\tilde{h}\rangle$ and $|\tilde{h}\tilde{g}\rangle$ can be sketched as $|\tilde{g}\tilde{h}\rangle \rightarrow |sp\rangle \rightsquigarrow |ps\rangle \rightarrow |\tilde{h}\tilde{g}\rangle$, where '$\rightarrow$' symbolizes a dressing laser-driven transition and '$\rightsquigarrow$' a state flip via dipole-dipole interactions. In total, the scheme allows for an interchange of ground states $|\tilde{g}\tilde{h}\rangle$ and $|\tilde{h}\tilde{g}\rangle$.

between two atoms 1 and 2, with

$$\tilde{V}_{12} = V_{nm}(r_{nm})\alpha^4 \left[\frac{1}{1 - [V_{nm}(r_{nm})/(2\hbar\Delta)]^2}\right]. \qquad (42)$$

Illustratively, one can think of the interaction (41) as arising from a three-step-process: In the first step, the ground states $|\,g\,\rangle$, $|\,h\,\rangle$ are excited to the Rydberg states $|\,s\,\rangle$, $|\,p\,\rangle$ by the dressing laser. In the second step, the dipole-dipole interactions flip the Rydberg states $|\,s\,\rangle$ and $|\,p\,\rangle$. In the final step, the Rydberg states are de-excited back to the respective ground states by the dressing field (see Fig. 6). This involves four photoinduced transitions in total, hence the interaction strength scales as α^4. As $\alpha \ll 1$, the interaction strength between dressed ground states is smaller than between pure excited states. However, the lifetime of dressed Rydberg states is larger than the one of actual Rydberg atoms [38].

Next, we will analyze these dressing-mediated interactions between two blocked clouds. We can distinguish two regimes in Eq. (42): For separations much smaller than the dipole-dipole blockade radius $r_{\text{dd}} \sim (V_0/2\hbar|\Delta|)^{1/3}$, the interactions are strongly suppressed. For separations much larger than r_{dd} we can simplify $\tilde{V}_{12} \approx \alpha^4 V_{12}$. For cloud widths $\sigma < r_{\text{dd}}$ and separations $L > r_{\text{dd}}$ we shall thus take $\tilde{V}_{12} = \alpha^4 V_{12}$ if atoms 1 and 2 reside in the same cloud, and $\tilde{V}_{12} = 0$ otherwise.

In the dressed case, we also have to modify the blockade radius for Van-der-Waals interactions, which prevent the simultaneous excitation of two s or two p states within one cloud, to $r_{\text{VdW}} \sim (C_6/2\hbar|\Delta|)^{1/6}$ [37]. The energy level shift of doubly Rydberg excited states, caused by Van-der-Waals interactions, renders the dressing field ineffective, if this shift exceeds the detuning. Further care has to be taken that this offset and the detuning do not counteract each other, i.e. we assume a red-detuned dressing laser if the interactions are repulsive and a blue-detuned dressing laser if the interactions are attractive.

Altogether we are led to an electronic Hamiltonian in the dressed case

$$H^{\text{d}}_{\text{el}}(\mathbf{R}) = \sum_{n\in\mathcal{A}, m\in\mathcal{B}} \tilde{V}_{nm}\; |\tilde{g}\rangle_n |\tilde{h}\rangle_m \langle\tilde{h}|_n \langle\tilde{g}|_m, \qquad (43)$$

which is a many-body version of (41) where no dressed interactions exist between atoms in the same cloud. This picture holds for $\alpha^2 N_{A,B} \lesssim 1$, otherwise our blockade assumption becomes inconsistent with the mean excited atom numbers $\alpha^2 N_{A,B}$ arising from the perturbative treatment in [38]. Since Eq. (43) conserves the total number of atoms in either dressed one-particle state, let us restrict the following discussion to the case of even N with equal numbers of atoms in $|\tilde{g}\rangle$ and $|\tilde{h}\rangle$, as well as equal numbers of atoms in the two clouds: $N_A = N_B = N_{\tilde{g}} = N_{\tilde{h}} \equiv N/2$. For the simplest non-trivial case $N = 4$ our basis contains the elements $\{|\tilde{g}\tilde{g} : \tilde{h}\tilde{h}\rangle, |\tilde{g}\tilde{h} : \tilde{g}\tilde{h}\rangle, |\tilde{g}\tilde{h} : \tilde{h}\tilde{g}\rangle, |\tilde{h}\tilde{g} : \tilde{g}\tilde{h}\rangle, |\tilde{h}\tilde{g} : \tilde{h}\tilde{g}\rangle, |\tilde{h}\tilde{h} : \tilde{g}\tilde{g}\rangle\}$, where the 2 entries before the colon label the one-particle-state of each atom in cloud A, while the 2 entries after the colon label the states of the atoms in cloud B. For general N, the number of basis states is given by the binomial coefficient $(N\;\; N/2)$.

In terms of the basis above, the matrix elements of the dressed electronic Hamiltonian (Eq. 43) are given by

$$H^{d}_{\text{el}} = \begin{pmatrix} 0 & \tilde{V}_{23} & \tilde{V}_{24} & \tilde{V}_{13} & \tilde{V}_{14} & 0 \\ \tilde{V}_{23} & 0 & 0 & 0 & 0 & \tilde{V}_{14} \\ \tilde{V}_{24} & 0 & 0 & 0 & 0 & \tilde{V}_{13} \\ \tilde{V}_{13} & 0 & 0 & 0 & 0 & \tilde{V}_{24} \\ \tilde{V}_{14} & 0 & 0 & 0 & 0 & \tilde{V}_{23} \\ 0 & \tilde{V}_{14} & \tilde{V}_{13} & \tilde{V}_{24} & \tilde{V}_{23} & 0 \end{pmatrix}. \qquad (44)$$

In contrast to the Hamiltonian of bare dipole-dipole interactions in table I, the one for dressed interactions (44) does not de-couple into blocks.

Just as in the case of "standard" dipole-dipole interactions, the electronic Hamiltonian $H^{\text{d}}_{\text{el}}(\mathbf{R})$ depends on the positions of the atoms, hence we again expect the interactions to give rise to motional dynamics. The full dressed Hamiltonian has the same form as in Eq. (2),

$$H^{\text{d}}(\mathbf{R}) = -\sum_{i=1}^{N} \frac{\hbar^2}{2M}\nabla^2_{r_i} + H^{\text{d}}_{\text{el}}(\mathbf{R}). \qquad (45)$$

To infer the motional dynamics resulting from (45), we consider the adiabatic energy surfaces defined in Eq. (14), i.e. the eigenvalues of $H^d_{\text{el}}(\mathbf{R})$:

$$\begin{aligned}
U_1(\mathbf{R}) &= 0, \\
U_2(\mathbf{R}) &= 0, \\
U_3(\mathbf{R}) &= \sqrt{(\tilde{V}_{14} - \tilde{V}_{23})^2 + (\tilde{V}_{13} - \tilde{V}_{24})^2}, \qquad (46) \\
U_4(\mathbf{R}) &= -\sqrt{(\tilde{V}_{14} - \tilde{V}_{23})^2 + (\tilde{V}_{13} - \tilde{V}_{24})^2}, \\
U_5(\mathbf{R}) &= \sqrt{(\tilde{V}_{14} + \tilde{V}_{23})^2 + (\tilde{V}_{13} + \tilde{V}_{24})^2}, \\
U_6(\mathbf{R}) &= -\sqrt{(\tilde{V}_{14} + \tilde{V}_{23})^2 + (\tilde{V}_{13} + \tilde{V}_{24})^2}.
\end{aligned}$$

In a regime where the atomic motion is adiabatic with respect to the energy scale defined by (46), the gradient of the $k-th$ eigenvalue with respect to the position r_i of the $i-th$ atom determines the force and hence motion of this atom [14–16],

$$F_i^k = -\partial_{r_i} U_k(\mathbf{R}). \qquad (47)$$

Let us for clarity's sake consider the special case where the distances between all atom pairs with atoms in different clouds are the same, i.e. $r_{13} = r_{14} = r_{23} = r_{24} \equiv \varrho$. Then the gradient of the eigenvalues U_5 and U_6 has the structure

$$\mathbf{F}^5 = \begin{pmatrix} \xi \\ \xi \\ -\xi \\ -\xi \end{pmatrix} = -\mathbf{F}^6, \qquad (48)$$

where $\xi = 3\sqrt{2}V_0\alpha^4/\varrho^4$ is the magnitude of the force. We see that the atoms in cloud A both experience the same force, as do both atoms in cloud B (with opposite sign). In other words, the dynamics on these two adiabatic surfaces corresponds to repulsion and attraction of the *whole* cloud. In the general case where the interatomic distances are not exactly the same (hence neither are the matrix elements $\tilde{V}_{ij}$) the magnitudes of the forces will slightly differ, which does not qualitatively change the picture as long as the spatial extension of each cloud is much smaller than the distance between the clouds. It is straightforward to extend the special case considered here to larger atom numbers, i.e. one can verify that there always exists an adiabatic surface that corresponds to motion of the whole cloud. This statement is corroborated in Fig. 7, where we show the time-dependence of the total atomic density for the case $N_A = N_B = 4$ calculated with Tully's algorithm, starting in a wholly repulsive electronic state. It is also demonstrated that the dynamics is essentially adiabatic, with a non-adiabatic population transfer to other surfaces of the order of 10^{-7}.

It is quite remarkable that the observed motional dynamics resembles collective behaviour, although the atoms within one cloud are non-interacting. This is due to the fact that all atoms in one cloud are initially located very close to each other and experience (almost) the same force.

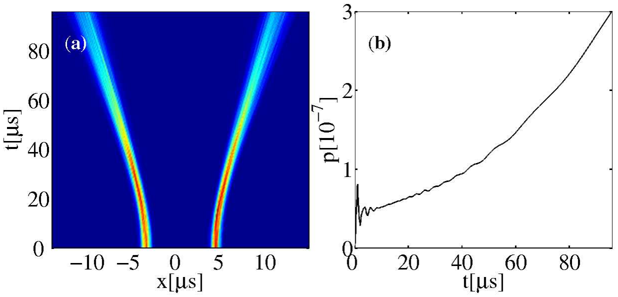

FIG. 7: Color online. Motion of dressed ground state atoms in a fully repulsive exciton state. (a): Total atom density as a function of time. Contrary to a superatom, the entire cloud of Rydberg-dressed ground state atoms is set in motion. (b): Non-adiabatic population transfer from the adiabatic surface on which the dynamics is initiated is of the order of 10^{-7}. The dynamics is shown for 8 atoms in total, with $N_A = N_B = 4$. The following parameters were used: $M = 12800\,\text{a.u.}$, $V_0 = 1.08 \cdot 10^6\,\text{a.u.}$, $\sigma = 0.5\,\mu\text{m}$, $L = 8\,\mu\text{m}$, $\Omega = 4\,\text{MHz}$, $\alpha = 0.18$.

VI. SUMMARY AND CONCLUSIONS

We studied the motion of two Rydberg-blockaded atom clouds, induced by their mutual resonant dipole-dipole interactions. On timescales where the kinetic energy of the atoms is still negligible, the dynamics in the electronic subspace exhibits superexponential dephasing. This behaviour can be very well described and understood within a mixed quantum classical framework, treating the nuclei as classical point particles and the electronic subspace as a discrete quantum system. For timescales on which the atomic motion is clearly visible, we observe that an initial coherent single excitation on each of the clouds (superatomic state) is physically removed by the dipole-dipole interactions. A single atom pair leaves the clouds, with the excitation being entirely localized on this pair. This finding may facilitate an experimental realization of quantum transport protocols in Rydberg aggregates, such as proposed in [13, 15] since one-atom-sites may be replaced by micro traps containing several atoms.

In the second part of the paper, we considered a modified setup where genuine Rydberg excitations were replaced by a weak Rydberg state admixture to ground states. In contrast to fragmenting superatoms, the laser-dressed ground state atoms remain grouped together, and the motion from dressed dipole-dipole interactions is seen for the whole cloud. This opens a new direction for the implementation of motional mesoscopic nonclassical states. Consider for example a scenario in which two such clouds are prepared in a superposition of collective attraction and repulsion. If interference upon recombination of the two quantum pathways could be observed, one would have demonstrated a quantum mechanical superposition which extends over several micrometers. Such a scheme presents a realization of an optically resolvable Schrödinger cat [49].

Appendix A: Herman-Kluk Propagator

In this appendix we simplify the Herman-Kluk propagator, Eq. (19), to arrive at the expression in Eq. (24), and elaborate on the conditions under which this simplification is valid.

The semi-classical trajectories encapsulating the frozen gas approximation are given by

$$\begin{aligned} \mathbf{q}_t &= \mathbf{q}', \\ \mathbf{p}_t &= \mathbf{p}' - \frac{\partial U(\mathbf{q}')}{\partial \mathbf{q}'}t, \end{aligned} \tag{A1}$$

where $\mathbf{q}', \mathbf{p}'$ are the initial phase space coordinates at $t' = 0$. Physically, this means that the atoms are too heavy to move on the timescale of interest, but there is nonetheless a build-up of momentum, which affects the phase. Let us first consider the prefactor C in the propagator (Eq. (21)). From the trajectories, we find the derivatives $\partial \mathbf{p}_t/\partial \mathbf{p}' = 1$, $\partial \mathbf{q}_t/\partial \mathbf{q}' = 1$, $\partial \mathbf{q}_t/\partial \mathbf{p}' = 0$, and $\partial \mathbf{p}_t/\partial \mathbf{q}' = -\partial^2 U^{\pm}(\mathbf{q}')/\partial {\mathbf{q}'}^2$. The prefactor therefore becomes

$$C = \left|\frac{1}{2}\left(2 + \frac{\sigma^2}{i\hbar}\frac{\partial^2 U^{\pm}(\mathbf{q}')}{\partial {\mathbf{q}'}^2}t\right)\right|^{1/2} \approx \left|1 \pm \frac{6V_0\sigma^2 t}{i\hbar L^5}\right|^{1/2}, \tag{A2}$$

where we used the adiabatic surfaces $U^{\pm}(\mathbf{q}') = \pm V_0/{\mathbf{q}'}^3$ and set $|\mathbf{q}'| \approx L$ after taking the derivative. On short timescales (cf. Eq. (22)), we can thus approximate the prefactor by unity. Furthermore, since the classical kinetic energy is, for the parameters of our setup on the given timescale, much smaller than the classical potential energy, we can approximate the action in the Herman-Kluk propagator as

$$S^{\pm}[\mathbf{q}_t, \mathbf{p}_t] \approx -U^{\pm}(\mathbf{q}')t. \tag{A3}$$

Finally, we insert the trajectories into the explicit form of the coherent states, used for the propagation, and carry out the momentum integration. This yields the following expression for the propagator:

$$\begin{aligned} K^{HK}(\mathbf{R}'', t; \mathbf{R}', t=0)^{\pm} &= \int d^N q' \, [\chi_N^{\sigma}(\mathbf{R}' - \mathbf{q}')]^2 \\ \times \exp\left[\frac{it}{\hbar}\left(U^{\pm}(\mathbf{q}') + \frac{\partial U^{\pm}(\mathbf{q}')}{\partial \mathbf{q}'}(\mathbf{R}'' - \mathbf{q}')\right)\right] &\delta(\mathbf{R}' - \mathbf{R}''), \end{aligned} \tag{A4}$$

where we used the property of the delta function $f(x)\delta(x-a) = f(a)\delta(x-a)$. The expression in the exponent is nothing but the first two terms of the Taylor-expansion of $U^{\pm}(\mathbf{R}'')$ around $\mathbf{R}'' = \mathbf{q}'$, which, in our case, is sufficient. Hence we replace the exponential by $\exp(-itU^{\pm}(\mathbf{R}'')/\hbar)$. The remaining integration over $\mathbf{q}'$ gives unity, according to the normalization of χ_N^{σ}. We thus arrive at the expression from Eq. (24).

Appendix B: Atomic motion from block-diagonal electronic Hamiltonians

In Section III, we have seen that the electronic Hamiltonian for a collection of Rydberg-blockaded atom clouds, Eq. (6), can be cast into a block-structure, where in each block only a single atom per cloud participates in non-trivial electronic dynamics. In this appendix we formally show that this leads to rapid entanglement of motion and electronic state, since in each block also only one atom per cloud performs non-trivial motional dynamics. This holds for any number of clouds and atoms per cloud. Further we show that non-adiabatic transitions do not affect this picture, as they respect the block structure. Let us consider the example of three clouds with two atoms each. The generalisation to other numbers is straightforward.

Let the atoms be grouped into clouds $\mathcal{A} = \{1, 2\}$, $\mathcal{B} = \{3, 4\}$, $\mathcal{C} = \{5, 6\}$. In that case the total Hamiltonian, including atomic motion and the electronic degrees of freedom, can be written as

$$H = \sum_{i=1}^{6} T_n + \mathrm{diag}[H_1, H_2, H_3, ...]. \tag{B1}$$

We abrreviated the kinetic energy term for each atom as $T_n = -\hbar^2\nabla_{r_n}^2/2M$. The symbol $\mathrm{diag}[H_1, H_2, H_3, ...]$ denotes a block-diagonal matrix, with 3×3 blocks $H_j(r_k, r_l, r_m)$. Crucially each block only depends on the coordinates of *three* atoms, with $k \in \mathcal{A}$, $l \in \mathcal{B}$, $m \in \mathcal{C}$, i.e. one from each cloud. The latin index j just numbers the blocks. Consequently, the time-evolution operator $\hat{U}(0, t) = \exp[-iHt/\hbar]$ also obtains a block-structure $\hat{U} = \mathrm{diag}[\hat{U}_1, \hat{U}_2, \hat{U}_3, ...]$, with

$$\begin{aligned} \hat{U}_j = &\exp\Big[-i\Big(\sum_{n \neq \{k,l,m\}} T_n\Big)t/\hbar\Big] \\ &\times \exp[-i(T_k + T_l + T_m + H_j(r_k, r_l, r_m))t/\hbar]. \end{aligned} \tag{B2}$$

We have used the operator hat on $\hat{U}$ here exclusively to avoid confusion with the potential energy surfaces U occuring elsewhere.

In Eq. (B2), the second exponential acts only on atoms k, l, m, while the pre-factor describes free motion of the remaining atoms. Now consider a time evolution beginning in an eigenstate of the electronic Hamiltonian H_{el} which will have support only in a single block j_0 of H. The form of $\hat{U}_j$ immediately tells us that three particles undergo dipole-dipole dynamics and the other ones perform free motion. Starting in a non-eigenstate will lead to quick entanglement of motion and electronic state, as in each block three j *different* particles participate in non-trivial dynamics. The block structure of $\hat{U}_j$ also immediately confirms the absence of non-adiabatic transitions between exciton states in different blocks. For an alternative argument, note that ∇H_{el} will have the same block-diagonal structure as H_{el}. From that we can see that non-adiabatic coupling terms, defined in the next appendix C in Eq. C3, vanish whenever the involved adiabatic eigenstates have support in different blocks.

Appendix C: Tully's algorithm

We start from the total Hamiltonian as given in Eqs. (2) or (B1). Tully's algorithm is implemented as follows. One first finds the adiabatic eigenstates in the electronic subspace $|\varphi_k(\mathbf{R})\rangle$ and the corresponding energies $U_k(\mathbf{R})$, and expands the wave function in this basis, cf. Eqs. (14) and (15). However, contrary to a full quantum mechanical approach, the expansion coefficients do not depend on the atomic positions, and here we denote them by $c_k(t)$ to underline the difference:

$$\Psi(\mathbf{R},t) = \sum_{k=1}^{2N_A N_B} c_k(t)|\varphi_k(\mathbf{R})\rangle. \tag{C1}$$

The adiabatic expansion is inserted into the time-dependent Schrödinger equation, which leads to a set of equations for the time-dependent expansion coefficients:

$$i\hbar\dot{c}_k = U_k c_k - i\hbar \sum_{j=1}^{2N_A N_B} \dot{\mathbf{R}}\cdot\mathbf{d}_{kj}c_j. \tag{C2}$$

In the above equation, we introduced non-adiabatic coupling vectors

$$\mathbf{d}_{kj} = \langle\varphi_k|\nabla_{\mathbf{R}}\varphi_j\rangle = \frac{\langle\varphi_k|\nabla_{\mathbf{R}}H_{\rm el}(\mathbf{R})|\varphi_j\rangle}{U_j(\mathbf{R})-U_k(\mathbf{R})}. \tag{C3}$$

Atomic motion is treated classically, i.e. the time evolution of the spatial degrees of freedom is obtained from a classical equation of motion (CEOM)

$$M\ddot{\mathbf{R}} = -\nabla_{\mathbf{R}}U_k(\mathbf{R}) \tag{C4}$$

and averaged over many trajectories. The averaging is performed such that the initial conditions for the CEOM, namely the position $\mathbf{R}(t=0)$, the velocity $\dot{\mathbf{R}}(t=0)$ and the adiabatic surface $k(t=0)$, resemble the Wigner distribution of the initial state. Then each trajectory is propagated on a single adiabatic surface k and the presence of non-adiabatic couplings $\mathbf{d}_{kj}$ is accounted for by introducing the possibility for instantaneous stochastic switches to another adiabatic surface j, as described in detail in Ref. [47].

Appendix D: Rydberg atoms moving through background gas

In Section IV, we argue that excitation and momentum transport in Rydberg aggregates, as described e.g. in Refs. [15, 16], should, in principle, be equally possible if single atom sites are replaced by atom clouds. To corroborate this claim, in what follows we estimate the impact of the processes that could potentially upset a dynamics such as sketched in Fig. 4. Let us consider Alkali atoms in an ultra-cold gas. They can be routinely excited to Rydberg states, and in general collisions with surrounding atoms do not necessarily lead to a loss of the excited state [50–52]. However, in the setup considered in Section IV, some Rydberg atoms are additionally accelerated within the gas due to the dipole-dipole interactions, with typical velocities of the order of $v_m = 4\,$m/s for the example of ^{7}Li. This is about two orders of magnitude larger than the thermal atomic velocity in an ultra-cold ^{7}Li gas at $T = 1\mu K$ of $v_T = 4.8\,$cm/s. However, as we estimate below, this does not lead to new regimes of atomic collisions. We consider the impact of the following processes: (i) Inelastic collisions of Rydberg and ground state atoms, (ii) elastic collisions of Rydberg and ground state atoms, and (iii) collisional ionization of Rydberg atoms.

(i) We can estimate the rate Γ_q of Rydberg state quenching collisions with background atoms, using $\Gamma_q = vn\sigma_q(\nu)$, where v is the velocity of the Rydberg atom with principal quantum number ν, n is the density of background atoms and $\sigma_q(\nu)$ is the cross section for the process. From [53] we have, e.g. for Rubidium atoms, $\sigma_q(40) = 2\times10^{-11}\,$cm^2. At $v = 4\,$m/s and with density $n = 1\times10^{18}\,$m^{-3} the inverse quenching rate is $\tau = 1/\Gamma_q = 125\,\mu$s, which is still larger than the Rydberg state lifetime $\tau = 46\mu$s. Note that for a scheme as depicted in Fig. 4 the effective background density would be an average over the intra- and intercloud regions and thus much smaller than the cloud peak density.

(ii) For elastic collisions, Ref. [54] gives a cross section of the order of $\sigma_{\rm el} \approx 10^4\,$a.u. $\approx 0.25\times10^{-12}\,$cm^2, which is about a factor of 80 smaller than the one given above for inelastic collisions. Elastic collisions are therefore even less important for the considered range of parameters.

(iii) In order to estimate the order of magnitude of the rate for collisional ionisation, we adopt an approximative formula derived by Lebedev [55]. For $\nu \gg l$, it reads, in atomic units,

$$\Gamma_{\rm ion} = \frac{8\sigma_{\rm el}T\nu_{\rm eff}}{\pi\mu}\exp\left(-\frac{1}{2\nu_{\rm eff}^2 T}\right), \tag{D1}$$

where $\sigma_{\rm el}$ is the cross section for elastic scattering of a Rydberg electron on a ground state atom, μ the reduced mass of the colliding system, T the temperature and $\nu_{\rm eff} = \nu-\delta_l$, δ_l being the quantum defect. In the ultracold regime, the low temperature of $\sim 1\mu$K $\approx 0.3\times10^{-11}$ a.u. leads to a vanishingly small exponent, making the collisional ionization absolutely negligible.

Acknowledgements

We thank Thomas Gallagher, Johannes Nipper, Cenap Ates, Thomas Pohl, Hanna Schempp and Christoph Hofmann for fruitful discussions. A.E. acknowledges support from the DFG under contract No. Ei 872/1-1.

[1] D. Jaksch, J. I. Cirac, P. Zoller, S. L. Rolston, R. Côté, and M. D. Lukin, Phys. Rev. Lett. **85**, 2208 (2000).

[2] M. S. Safronova, C. J. Williams, and C. W. Clark, Phys. Rev. A **67**, 040303 (2003).

[3] M. Saffman and K. Mølmer, Phys. Rev. Lett. **102**, 240502 (2009).

[4] M. Saffman, T. G. Walker, and K. Mølmer, Rev. Mod. Phys. **82**, 2313 (2010).

[5] L. Isenhower, E. Urban, X. L. Zhang, A. T. Gill, T. Henage, T. A. Johnson, T. G. Walker, and M. Saffman, Phys. Rev. Lett. **104**, 010503 (2010).

[6] K. J. Weatherill, J. D. Pritchard, R. P. Abel, M. G. Bason, A. K. Mohapatra, and C. S. Adams, J. Phys. B **41**, 201002 (2008).

[7] J. D. Pritchard, D. Maxwell, A. Gauguet, K. J. Weatherill, M. P. A. Jones, and C. S. Adams, Phys. Rev. Lett. **105**, 193603 (2010).

[8] C. Ates, S. Sevincli, and T. Pohl, Phys. Rev. A **83**, 041802 (2011).

[9] F. Yamaguchi, P. Milman, M. Brune, J. M. Raimond, and S. Haroche, Phys. Rev. A **66**, 010302 (2002).

[10] W. L. Yang, C. Y. Chen, and M. Feng, Phys. Rev. A **76**, 054301 (2007).

[11] C. Guerlin, E. Brion, T. Esslinger, and K. Mølmer, Phys. Rev. A **82**, 053832 (2010).

[12] S. Westermann, T. Amthor, A. L. de Oliveira, J. Deiglmayr, M. Reetz-Lamour, and M. Weidemüller, Eur. Phys. J. D **40**, 37 (2006).

[13] O. Mülken, A. Blumen, T. Amthor, C. Giese, M. Reetz-Lamour, and M. Weidemüller, Phys. Rev. Lett. **99**, 090601 (2007).

[14] C. Ates, A. Eisfeld, and J. M. Rost, New J. Phys. **10**, 045030 (2008).

[15] S. Wüster, C. Ates, A. Eisfeld, and J. M. Rost, Phys. Rev. Lett. **105**, 053004 (2010).

[16] S. Möbius, S. Wüster, C. Ates, A. Eisfeld, and J. M. Rost, J. Phys. B **44**, 184011 (2011).

[17] T. Holstein, Annals of Physics **8**, 325 (1959).

[18] A. Eisfeld and J. S. Briggs, Chem. Phys. **281**, 61 (2002).

[19] M. D. Lukin, M. Fleischhauer, R. Cote, L. M. Duan, D. Jaksch, J. I. Cirac, and P. Zoller, Phys. Rev. Lett. **87**, 037901 (2001).

[20] D. Tong, S. M. Farooqi, J. Stanojevic, S. Krishnan, Y. P. Zhang, R. Côté, E. E. Eyler, and P. L. Gould, Phys. Rev. Lett. **93**, 063001 (2004).

[21] K. Singer, M. Reetz-Lamour, T. Amthor, L. G. Marcassa, and M. Weidemüller, Phys. Rev. Lett. **93**, 163001 (2004).

[22] F. Robicheaux and J. V. Hernández, Phys. Rev. A **72**, 063403 (2005).

[23] T. Vogt, M. Viteau, A. Chotia, J. Zhao, D. Comparat, and P. Pillet, Phys. Rev. Lett. **99**, 073002 (2007).

[24] R. Heidemann, U. Raitzsch, V. Bendkowsky, B. Butscher, R. Löw, L. Santos, and T. Pfau, Phys. Rev. Lett. **99**, 163601 (2007).

[25] C. Ates, T. Pohl, T. Pattard, and J. M. Rost, Phys. Rev. Lett. **98** (2007).

[26] E. Urban, T. A. Johnson, T. Henage, L. Isenhower, D. D. Yavuz, T. G. Walker, and M. Saffman, Nat. Phys. **5**, 110 (2009).

[27] A. Gaëtan, Y. Miroshnychenko, T. Wilk, A. Chotia, M. Viteau, D. Comparat, P. Pillet, A. Browaeys, and P. Grangier, Nat. Phys. **5**, 115 (2009).

[28] M. Viteau, M. G. Bason, J. Radogostowicz, N. Malossi, D. Ciampini, O. Morsch, and E. Arimondo, Phys. Rev. Lett. **107**, 060402 (2011).

[29] T. J. Carroll, C. Daniel, L. Hoover, T. Sidie, and M. W. Noel, Phys. Rev. A **80**, 052712 (2009).

[30] F. Robicheaux and J. V. Hernández, Phys. Rev. A **72**, 063403 (2005).

[31] V. Vuletic, Nature Phys. **2**, 801 (2006).

[32] W. R. Anderson, J. R. Veale, and T. Gallagher, Phys. Rev. Lett. **80**, 249 (1998).

[33] F. Robicheaux, J. V. Hernandez, T. Topcu, and L. D. Noordam, Phys. Rev. A **70**, 042703 (2004).

[34] W. Li, P. J. Tanner, and T. Gallagher, Phys. Rev. Lett. **94**, 173001 (2005).

[35] L. Santos, G. V. Shlyapnikov, P. Zoller, and M. Lewenstein, Phys. Rev. Lett. **85**, 1791 (2000).

[36] M. Müller, L. Liang, I. Lesanovsky, and P. Zoller, New J. Phys. **10**, 093009 (2008).

[37] N. Henkel, R. Nath, and T. Pohl, Phys. Rev. Lett **104**, 053004 (2010).

[38] S. Wüster, C. Ates, A. Eisfeld, and J. M. Rost, New J. Phys. **13**, 073044 (2011).

[39] H. Park, P. J. Tanner, B. J. Claessens, E. S. Shuman, and T. F. Gallagher, Phys. Rev. A **84**, 022704 (2011).

[40] M. L. Wall, F. Robicheaux, and R. R. Jones, J. Phys. B **40**, 3693 (2007).

[41] W. Domcke, D. R. Yarkony, and H. Köppel, *Conical Intersections* (World Scientific, 2004).

[42] E. Kluk, M. F. Herman, and H. L. Davis, J. Chem. Phys. **84**, 326 (1986).

[43] F. Grossmann and A. L. Xavier Jr., Phys. Lett. A **243**, 243 (1998).

[44] F. Grossmann and M. F. Herman, J. Phys. A **35**, 9489 (2002).

[45] F. Grossmann, *Theoretical Femtosecond Physics* (Springer, 2008).

[46] J. C. Tully and R. K. Preston, J. Chem. Phys. **55**, 562 (1971).

[47] J. C. Tully, J. Chem. Phys. **93**, 1061 (1990).

[48] S. Hammes-Schiffer and J. C. Tully, J. Chem. Phys. **101**, 4657 (1994).

[49] S. Möbius, M. Genkin, A. Eisfeld, S. Wüster, and J. M. Rost (to be published).

[50] S. S. Kano, Y. Taira, H. Takuma, K. Nishizawa, and K. Sakurai, Phys. Rev. A **32**, 1914 (1985).

[51] A. Walz-Flannigan, J. R. Guest, J.-H. Choi, and G. Raithel, Phys. Rev. A **69**, 063405 (2004).

[52] J.-H. Choi, J. R. Guest, A. P. Povilus, E. Hansis, and G. Raithel, Phys. Rev. Lett. **95**, 243001 (2005).

[53] M. Hugon, F. Gounand, P. R. Fournier, and J. Berlande, J. Phys. B **16**, 2531 (1983).

[54] B. Kaulakys and V. Svedas, J. Phys. B **20**, L565 (1987).

[55] V. S. Lebedev, J. Phys. B **24**, 1977 (1991).